# The flow in a cylindrical container with a rotating end wall at small but finite Reynolds number

Benson K. Muite[a)]
*School of Engineering and Applied Science, Princeton University, Princeton, New Jersey 08544*

(Received 21 October 2003; accepted 16 June 2004; published online 20 August 2004)

Similarity solutions of the first kind are intermediate asymptotic solutions for the Stokes flow field and for the first-order inertial correction to the Stokes flow field in small aspect ratio geometries with both no-slip and free-slip boundary conditions opposite the rotating end wall. These results differ from the semi-infinite cylindrical container, where similarity solutions of the second kind are intermediate asymptotic representations of the Stokes and first-order flow fields. Lanczos factors are used to show that for Reynolds numbers less than 1, the boundary discontinuity has a limited influence on the flow field with a no-slip boundary condition opposite the rotating end wall but the boundary discontinuity is important in determining the flow field with a free-slip boundary condition opposite the rotating end wall. © *2004 American Institute of Physics*. [DOI: 10.1063/1.1779567]

## I. INTRODUCTION

The flow in a cylindrical container with a rotating end wall (see Fig. 1) is well studied because it exhibits vortex breakdown[1–5] that is dependent on the Reynolds number and aspect ratio, $\gamma=H^*/r_o^*$ (where $H^*$ is the length of the container and $r_o^*$ its radius). Two geometries have been studied, one with a stationary solid surface opposite the rotating end wall,[1,2] and the other with a free surface opposite the rotating end wall.[2] In both geometries, the dominant velocity component is azimuthal. There is also a secondary axial and radial flow. For aspect ratios close to 1, this secondary flow consists of fluid that leaves the upper rotating lid, travels down the stationary sidewall, moves in along the bottom wall, and finally returns up along the center of the cavity. When the Reynolds number is greater than 1000 with a fixed upper surface, or greater than 500 with a free surface, and the aspect ratio is between 1 and 2, experiments show that the eddy pattern that exists at lower Reynolds numbers is modified.[1–4] Along the central axis of the cavity, the secondary flow has a stagnation point. After the stagnation point follows a bubblelike region with circulation in the axial and radial planes which is in the opposite direction to circulation in the rest of the cavity.

The flow in the geometry with a fixed end wall opposite the rotating end wall has also been extensively studied for small aspect ratio and arbitrary Reynolds number. This flow is of scientific interest because it admits similarity solutions that satisfy all experimentally realistic boundary conditions except those at the stationary sidewall[6,7] and because for Reynolds numbers significantly greater than 1, the similarity solution has multiple stable solution branches.[6,7]

The primary purpose of the present study is to understand the dominance of particular and complementary solutions in the Stokes flow and the first-order inertial correction to the Stokes flow in a cylindrical cavity with a rotating end wall for both free surface and no-slip boundary conditions opposite the rotating end wall. To accomplish this objective, the asymptotic behavior of analytical flow field solutions is derived. The secondary purpose is to obtain a qualitative understanding of the effect of discontinuous boundary conditions on the torque and the flow fields. To accomplish this objective, Lanczos factors are introduced to allow differentiation of the series solutions for the Stokes flow field. It should be noted that because a qualitative and theoretical understanding is desired, simplifications are made to allow for analytical solutions that asymptotically describe the flow fields away from the stationary sidewall for small aspect ratios. This is not a review, and because extensive research has been performed on rotating disk flows only those studies that are directly relevant to this particular investigation will be mentioned.

Schmeiden[8] has used exact Stokes solutions to show that the discontinuous boundary conditions imply a logarithmically divergent torque. Panton[9] has found a perturbation solution for the Stokes flow field in a short aspect ratio geometry. Khalili and Rath[10] have also investigated exact Stokes flow solutions for the cylindrical cavity with a rotating end wall. Pao[11,12] experimentally and numerically verified that the analytical Stokes solution described the azimuthal flow for Reynolds numbers less than 10. Schulz-Grunow[13] determined polynomial solutions for the Stokes flow and the first-order inertial correction to the Stokes flow in a small aspect ratio cylindrical cavity with a rotating end wall. None of these studies analytically examines the effect of satisfying the no-slip boundary conditions on the stationary sidewall for the first-order axial and radial fluid motions, and none of these studies has considered the Stokes flow with a free surface opposite the rotating end wall.

Azerad and Bänsch[14] studied the flow in a cone and plate rheometer. This flow is similar to that considered here except that instead of a rotating end wall, there is a rotating cone with a tip that extends to the flat stationary end wall of the cavity. This geometry also has a boundary discontinuity that Azerad and Bänsch[14] prove is unimportant in determining

[a)]Electronic mail: benson_muite@yahoo.com

 

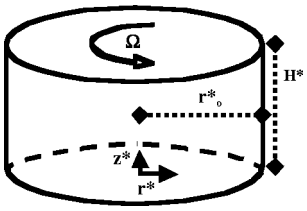


FIG. 1. A cylindrical cavity with a rotating end wall.

the global low Reynolds number flow field except near the discontinuity. They give evidence in support of their proof from simulations and experiments. In many other simulations of driven cavity flows with discontinuities, the effect of the discontinuity on the accuracy of the simulation away from the discontinuity is negligible for Reynolds numbers less than 1.[15] However, in many of these cases it is difficult to use analytical Stokes flow field solutions to explicitly understand the effect of the discontinuity on the first-order inertial correction because the resulting series diverges when differentiated. In the present study, it is shown that it is possible to transform the series so that it converges and can then indicate the effect of the discontinuity on the flow field.

The first-order inertial correction calculated in this study is very similar to a two-dimensional flow in a lid driven cavity. Shankar and Deshpande[15] summarize the characteristics of these flows. When inertial effects are important, only numerical solutions have been obtained. However, it is possible to obtain analytical and quasianalytical solutions for arbitrary boundary conditions in the Stokes limit.[15,16] In the present study, the method of homogeneous solutions is extended to obtain approximate analytical solutions with weak inertial effects. This approach complements the numerous full numerical simulations of the flow.[11,12,17–23]

Spohn *et al.*,[2,3] Lopez *et al.*,[17] Brons *et al.*,[24] and Hirsa *et al.*[25] have studied the flow in a cylindrical container with a free surface opposite the stationary end wall. In these studies, good agreement is only obtained between computations and experiments for aspect ratios greater than a half. In particular, for Reynolds numbers greater than 1, Lopez *et al.*[17] show that at small aspect ratio, the boundary conditions on the free surface are important in determining the symmetries of the primary instability. Spohn *et al.*[3] also observe that the flow structure at small aspect ratios is very sensitive to perturbations. This motivates the question of what is special about small aspect ratios that makes these flows difficult to compute.

Using a regular perturbation scheme in the Reynolds number, Hills[26] studied the first-order effects of inertia in a circular semi-infinite lid-driven cavity. Hills[26] found that because the zeroth-order flow field is azimuthal, the first-order inertial correction has a defining role in the axial and radial flow fields: he shows that it creates an infinite sequence of vortices that decay exponentially with distance from the rotating end wall. The structure of the infinite sequence of vortices is determined by the slowest axially decaying solution of the homogeneous equation, which dominates over the particular solution away from the rotating lid (a similarity solution of the second kind[27]). However, experiments can only be done in finite size cavities, and thus it is important to understand the effect of an additional boundary.

Following this introduction, the governing equations are obtained and scaled in Sec. II. The flow fields are solved for in Sec. III. The perturbation scheme used is described in Sec. III A. Exact Stokes solutions and intermediate asymptotic Stokes solutions are obtained in Sec. III B. In Sec. III C, Lanczos factors are used to accelerate the rate of convergence of the series solutions, and in Sec. III D, Lanczos factors are used to examine the effect of the discontinuity on the forcing function for the first-order inertial correction. In Sec. III E, a quasianalytical solution for the secondary flow field is obtained by using the approximate intermediate asymptotic similarity solution for a small aspect ratio geometry with a fixed end wall opposite the rotating end wall. The dominant asymptotic secondary flow structure for a geometry with a free-slip boundary condition opposite the rotating end wall is determined in Sec. III F. Lanczos factors are used to examine the effect of discontinuous boundary conditions on the torque in Sec. III G. Finally, in Sec. IV, the results of this study are discussed in light of previous studies.

## II. GOVERNING EQUATIONS

The flow of an incompressible fluid in a cylindrical lid-driven cavity is modeled by the steady state Navier–Stokes equations with no-slip boundary conditions which, assuming cylindrical symmetry, are in the dimensionless azimuthal velocity–stream function form:

$$\mathrm{Re}\left(\frac{1}{r\gamma}\frac{\partial\Psi}{\partial r}\frac{\partial u_\theta}{\partial z}-\frac{1}{r\gamma}\frac{\partial\Psi}{\partial z}\frac{\partial u_\theta}{\partial r}-\frac{u_\theta}{\gamma r^2}\frac{\partial\Psi}{\partial z}\right)$$
$$=\frac{1}{\gamma^2}\frac{\partial^2 u_\theta}{\partial z^2}+\frac{1}{r}\frac{\partial u_\theta}{\partial r}+\frac{\partial^2 u_\theta}{\partial r^2}-\frac{u_\theta}{r^2},$$

$$\mathrm{Re}\left[2\frac{u_\theta}{r\gamma}\frac{\partial u_\theta}{\partial z}-\frac{1}{r^3\gamma}\frac{\partial\Psi}{\partial r}\frac{\partial^2\Psi}{\partial z\partial r}+\frac{1}{r^3\gamma}\frac{\partial\Psi}{\partial z}\left(\frac{3}{r}\frac{\partial\Psi}{\partial r}-\frac{2}{\gamma^2}\frac{\partial^2\Psi}{\partial z^2}\right.\right.$$
$$\left.\left.-\frac{\partial^2\Psi}{\partial r^2}\right)\right]=D^2D^2\Psi, \tag{1}$$

where the operator $D^2$ is

$$D^2=r\frac{\partial}{\partial r}\left(\frac{1}{r}\frac{\partial}{\partial r}\right)+\frac{1}{\gamma^2}\frac{\partial^2}{\partial z^2}.$$

In this formulation, the gravitational and pressure terms are eliminated by cross differentiation of the axial and radial momentum equations. The velocities are found using the following relations:

$$u_r=\frac{-1}{\gamma r}\frac{\partial\Psi}{\partial z},\quad u_z=\frac{1}{r}\frac{\partial\Psi}{\partial r}. \tag{2}$$

With one fixed end wall, the no-slip boundary conditions are

$$u_\theta[r,1]=r,\quad u_\theta[r,0]=u_\theta[1,z]=0,$$

$$\frac{\partial\Psi}{\partial r}[r,1]=\frac{\partial\Psi}{\partial r}[r,0]=\frac{\partial\Psi}{\partial r}[1,z]=0, \tag{3}$$

$$\frac{\partial \Psi}{\partial z}[r,1] = \frac{\partial \Psi}{\partial z}[r,0] = \frac{\partial \Psi}{\partial z}[1,z] = 0.$$

With a free surface, the boundary condition $u_\theta[r,0] = \partial \Psi / \partial z[r,0] = 0$ is replaced by $\partial u_\theta / \partial z[r,0] = \partial^2 \Psi / \partial z^2[r,0] = 0$. As discussed by Brons *et al.*,[24] a flat and free-slip boundary condition is only appropriate at low Froude numbers for fluids with clean surfaces where the effects of gravity and surface tension can be neglected.

The symbols in these equations are

$$z = z^*/H^*,\ r = r^*/r_o^*,\ u_\theta = u_\theta^*/\overline{u_\theta}^*,$$

$$\overline{u_\theta}^* = r_o^* \Omega^*,\ u_r = u_r^*/\overline{u_\theta}^*,\ u_z = u_z^*/\overline{u_\theta}^*,$$

$$\gamma = H^*/r_o^*,\ \Psi = \Psi^*/r_o^{*2}\Omega^*,\ \mathrm{Re} = \overline{u_\theta}^* r_o^*/\nu^*.$$

The dimensional quantities have an asterisk and are $z^*$, the axial distance; $r^*$, the radial distance; $r_0^*$, the radius of the cavity; $\mu^*$, the dynamic viscosity of the fluid in the cavity, $\Omega^*$, the angular velocity of the rotating lid; $\Psi^*$ the stream function; and $\upsilon^*$, the kinematic viscosity of the fluid in the cavity. The scaling speed $\overline{u_\theta}^*$ is the speed of the edge of the rotating lid. The scaling lengths are the radius and height of the cavity, $r_0^*$ and $H^*$, respectively. For ease of computation the velocity transition between the stationary sidewall and the rotating end wall is modeled as a sudden jump, although in an experiment there is likely to be a small gap.

## III. SOLUTION

### A. Perturbation expansion

An asymptotic expansion in Reynolds number, as used by Hills,[26] is used to calculate the flow,

$$u_\theta = u_{\theta,0} + \mathrm{Re}\, u_{\theta,1} + \mathrm{Re}^2 u_{\theta,2} + \cdots,$$
$$\Psi = \Psi_0 + \mathrm{Re}\, \Psi_1 + \mathrm{Re}^2 \Psi_2 + \cdots. \tag{4}$$

Substituting these expressions into the Navier–Stokes equations and matching the equations and the boundary conditions order by order in the Reynolds number, the linear partial differential equations to be solved at each order are obtained.

The zeroth-order Stokes flow field has only an azimuthal component and satisfies

$$\frac{1}{\gamma^2}\frac{\partial^2 u_{\theta,0}}{\partial z^2} + \frac{1}{r}\frac{\partial u_{\theta,0}}{\partial r} + \frac{\partial^2 u_{\theta,0}}{\partial r^2} - \frac{u_{\theta,0}}{r^2} = 0,\ \ \Psi_o = 0. \tag{5}$$

The no-slip boundary conditions for this flow field are

$$u_{\theta,0}[r,1] = r,\ \ u_{\theta,0}[r,0] = u_{\theta,0}[1,z] = 0. \tag{6}$$

With a free surface, the no-slip boundary condition, $u_{\theta,0}[r,0]=0$, becomes a free-slip boundary condition, $\partial u_{\theta,0}/\partial z[r,0]=0$. In this Stokes equation, the azimuthal velocity field is uncoupled from the zero axial and radial velocity fields.

The first-order correction flow field satisfies

$$\frac{1}{\gamma}\frac{\partial u_{\theta,0}^2}{\partial z} = D^2 D^2 \Psi_1,\ u_{\theta,1} = 0. \tag{7}$$

With a stationary end wall, the first partial derivatives of the stream function are zero on all walls of the cavity. With a free surface, the flow field also has null boundary conditions except at the free surface, where the axial partial derivatives of the azimuthal and radial velocities are zero. At first order, the azimuthal velocity field is again uncoupled from the stream function. In comparison to the zeroth-order flow, the first-order azimuthal velocity field has no forcing term and is zero.

A regular perturbation expansion requires that throughout the flow field, $|\mathbf{u}_n| \gg |\mathbf{u}_{n+1}|$ and $|\mathbf{u}_n| \gg \mathrm{Re}\,|\mathbf{u}_n \cdot \nabla \mathbf{u}_n|$. In a regular perturbation expansion, these magnitude requirements are met by scaling the velocities and distances appropriately. When this scaling cannot be accomplished throughout the domain, a singular perturbation solution is required and the regular perturbation solution is not uniformly valid.

### B. Stokes flow solutions

It will be assumed that the Stokes flow field has azimuthal symmetry and so only depends on the radial and axial coordinates. Therefore, the solution automatically satisfies the continuity equation. With a fixed end wall opposite the rotating end wall, the solution $u_{\theta,0,fix}$ is found using a polynomial similarity solution obtained by Schulz-Grunow,[13] $rz$, and then satisfying the no-slip boundary condition by using separation of variables. The calculation method used to obtain this solution is demonstrated in Appendix A for a flow with a free-slip boundary condition opposite the rotating end wall, the final solution is

$$u_{\theta,0,fix} = rz + 2\sum_{n=1}^{\infty} \frac{\sin[n\pi(z-1)]}{n\pi} \frac{I_1[n\pi r/\gamma]}{I_1[n\pi/\gamma]}, \tag{8}$$

where $I_m$ is the modified Bessel function of the $m$th kind. As explained by Deen[28] an alternative series representation of the unique solution can be found by using a series expansion in a different direction. Such a solution is useful for comparing the results obtained in the present study to results obtained by Hills.[26] Schmeiden[8] and Pao[12] have obtained such an alternative solution,

$$u_{\theta,0,fix} = \sum_{n=1}^{\infty} \frac{-2\sinh[\gamma z \lambda_n]}{\lambda_n \sinh[\gamma \lambda_n]} \frac{J_1[\lambda_n r]}{J_0[\lambda_n]}, \tag{9}$$

where $J_m$ is the regular Bessel function of the $m$th kind and $\lambda_n$ is the $n$th zero of $J_1$. Equation (8) is plotted for aspect ratios of 0.25, 1, and 4 in Figs. 2(a)–2(c), respectively, using a 100-term expansion. This series satisfied the boundary conditions everywhere to within 0.02 except at the corner discontinuity where there was an overshoot of 0.2 because of the Gibbs oscillations. The figures show that for a large aspect ratio, the azimuthal flow is concentrated in a region near the rotating wall, whereas for a small aspect ratio the azimuthal flow has a uniform axial velocity gradient.

The series expressions for the azimuthal velocity field are complicated. To compute an analytical approximation for

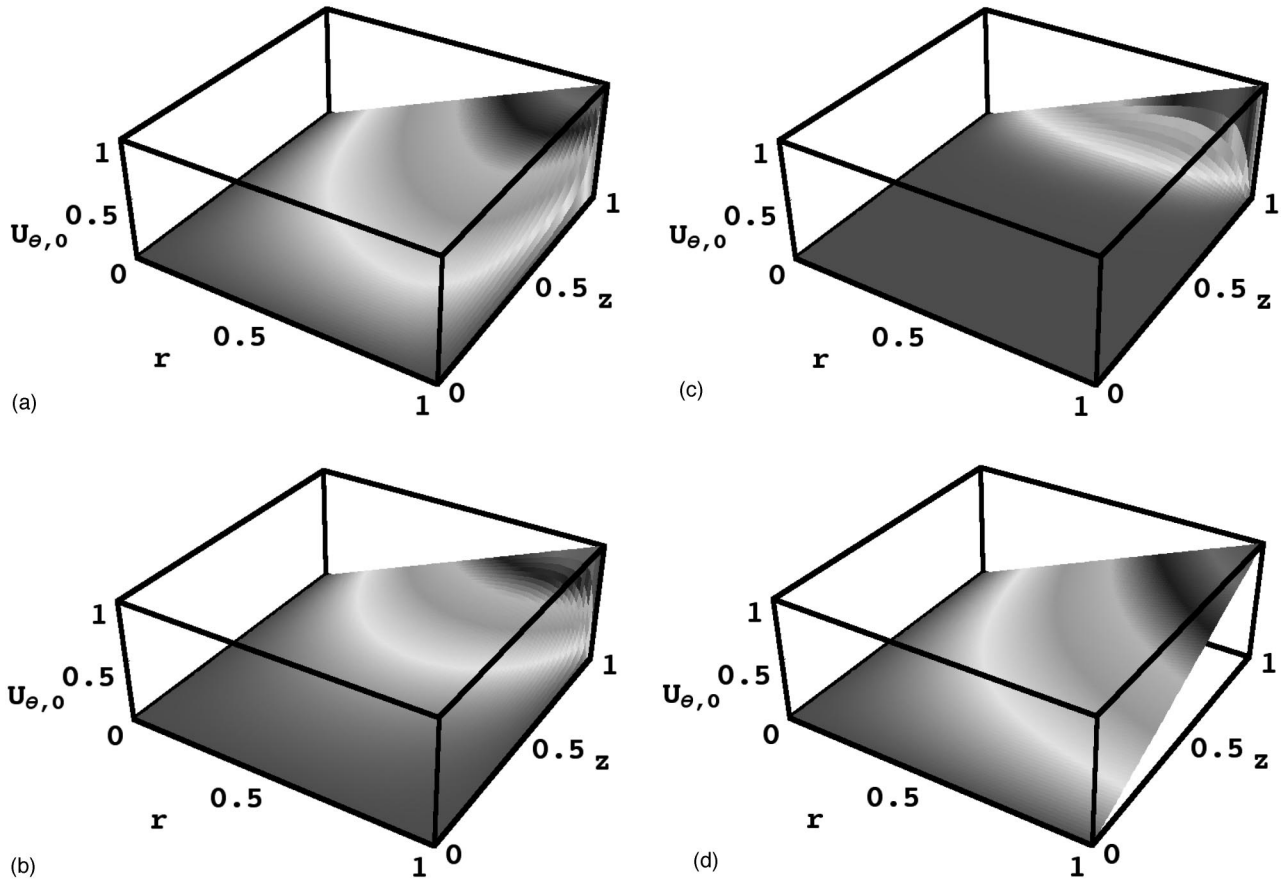


FIG. 2. (a) Stokes solution for an aspect ratio $\gamma=0.25$ with a stationary end wall. (b) Stokes solution for an aspect ratio $\gamma=1$ with a stationary end wall. (c) Stokes solution for an aspect ratio $\gamma=4$ with a stationary end wall. (d) A plot of the small aspect ratio similarity solution $rz$.

the first inertial correction, a simpler expression is required. Figure 2(d) shows the first part, $rz$, of the solution for the azimuthal velocity field in an apparatus with one stationary end wall in Eq. (8). By comparing Fig. 2(a) to Fig. 2(d), one observes that as found by Panton[9] and Pao[12] the expression $rz$ is a good approximate representation of the Stokes velocity field for a small aspect ratio geometry with a stationary end wall.

To obtain the Stokes solution with a free surface, $u_{\theta,0,free}$, a correction series is added to $r$, the solution for solid body rotation, to satisfy the no-slip boundary condition at the outer stationary wall. The series is found using separation of variables as demonstrated in Appendix A; the full solution is

$$u_{\theta,0,free} = r + 2\sum_{n=0}^{\infty} \frac{I_1[(n+1/2)\pi r/\gamma]}{I_1[(n+1/2)\pi/\gamma]} \frac{\sin[(n+1/2)\pi(z-1)]}{(n+1/2)\pi}. \tag{10}$$

As shown in Appendix A, an alternative series representation of this solution can also be found and is

$$u_{\theta,0,free} = \sum_{n=1}^{\infty} \frac{-2}{\lambda_n} \frac{\cosh[\gamma z \lambda_n]}{\cosh[\gamma \lambda_n]} \frac{J_1[\lambda_n r]}{J_0[\lambda_n]}. \tag{11}$$

This solution is plotted for aspect ratios of 0.25, 1, and 4 in Figs. 3(a)–3(c), respectively, using a 100-term expansion. With a free surface and at small aspect ratio, the fluid is in solid body rotation away from the sidewalls. This solid body rotation similarity solution is a good approximation to the flow field at small aspect ratio and small Reynolds number everywhere except near the stationary sidewalls. At large aspect ratio, Fig. 3(c), the solution with a free surface is similar to the solution with a fixed end wall, Fig. 2(c).

### C. Accelerating convergence of the Stokes flow field series expansions using Lanczos factors

It is well known that discontinuous boundary conditions slow down the rate of convergence of series solutions.[29,30] Furthermore, to obtain a physically reasonable solution for the velocity field, the conditions at the corner cannot be modeled using a jump discontinuity. This is because in any physical situation, there will be an imposed length scale appropriate to the corner; this could be a balance between viscous and inertial forces, a balance between surface tension and viscous forces, the gap between the rotating and stationary walls, or a Knudsen length scale because the continuum assumption no longer holds. It is therefore appropriate to modify the series expansions for the velocity field to reflect a minimum resolvable scale.

A minimum resolvable scale can be imposed by truncating the series representation. Simple truncation does not ensure that the resulting series gives an accurate representation of the flow field. In a trigonometric expansion, a procedure

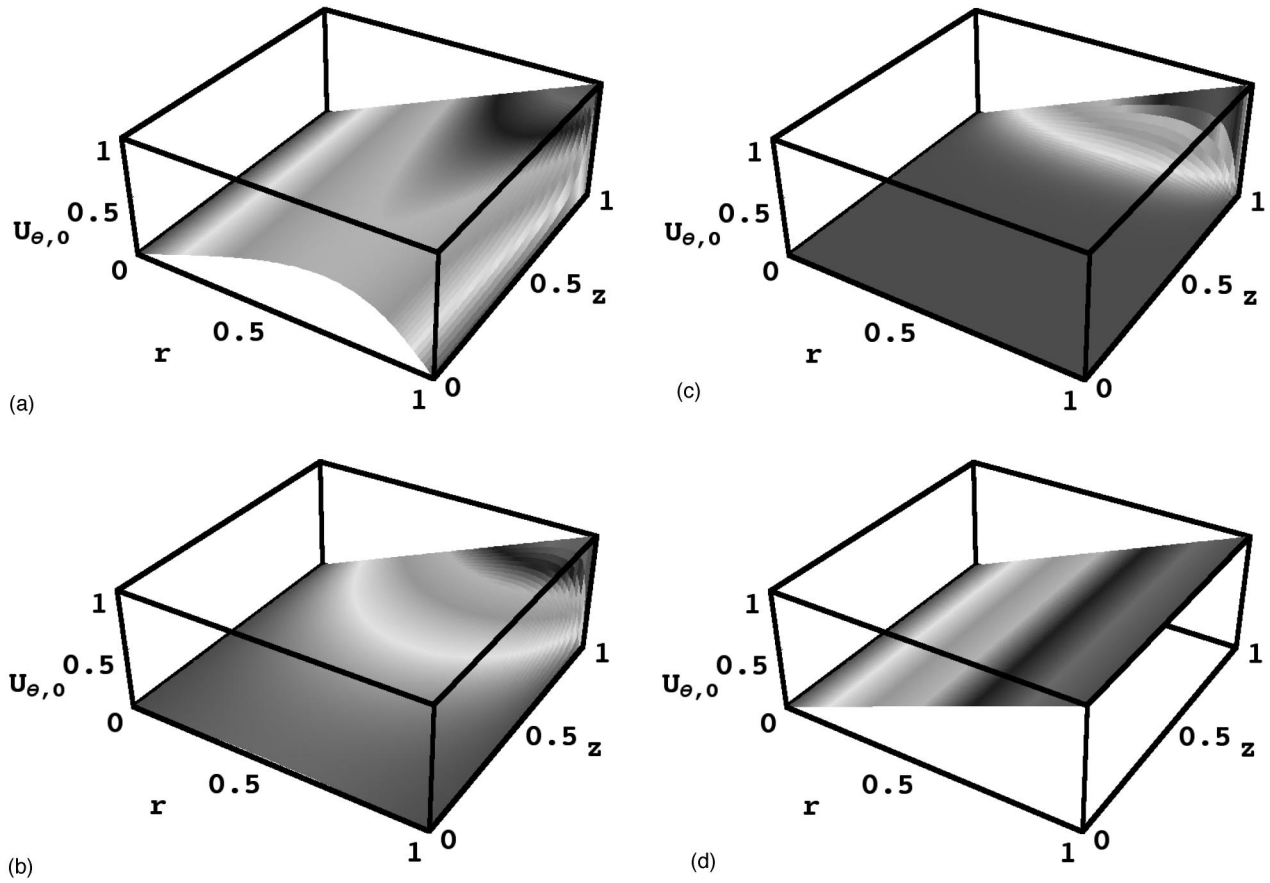


FIG. 3. (a) Stokes solution for an aspect ratio $\gamma=0.25$ with a free surface. (b) Stokes solution for an aspect ratio $\gamma=1$ with a free surface. (c) Stokes solution for an aspect ratio $\gamma=4$ with a free surface. (d) A plot of the solid body rotation similarity solution, $r$.

that results in a truncated series expansion, which approximates the required function, is the application of Lanczos correction factors to the original trigonometric expansion.[31,30] These factors replace the discontinuous jump in velocity, with a rapid transition region, which still preserves the properties of the solution away from the discontinuity. The resulting velocity fields are

$$u_{\theta,0,fix} = rz + 2\sum_{n=1}^{k} \frac{\sin[n\pi(z-1)]}{n\pi} \frac{I_1[n\pi r/\gamma]}{I_1[n\pi/\gamma]} \frac{\sin[n\pi/k]}{n\pi/k}, \tag{12}$$

and

$$u_{\theta,0,free} = r + 2\sum_{n=0}^{k} \frac{I_1[(n+1/2)\pi r/\gamma]}{I_1[(n+1/2)\pi/\gamma]} \times \frac{\sin[(n+1/2)\pi(z-1)]}{(n+1/2)\pi} \frac{\sin[(n+1/2)\pi/k]}{(n+1/2)\pi/k}, \tag{13}$$

where the index $k$ denotes the largest resolvable wave number. For $k>15$, there was very little difference between the Lanczos modified series and the Fourier series expansion with 50 or more terms everywhere except at the boundary discontinuity. Using 30 terms in the series expansion, the Lanczos modified series had a maximum overshoot of 0.025 at the corner discontinuity and satisfied the boundary conditions everywhere else to within 0.005. The Lanczos modified series provides a more accurate representation of the velocity field with fewer terms than the Fourier series expansions. Lanczos showed similar results for the expansions of functions of a single variable.[31] There are alternative methods of implementing a velocity transition region such as a boundary layer function[29] or a small gap with a free surface[8] or an averaged velocity transition region in a basis not composed of trigonometric functions.[30] Such methods often result in complicated series expansion coefficients and so are not desirable methods for obtaining analytic solutions.

### D. Forcing function for the first-order inertial correction in a small aspect ratio geometry

The analysis in this section shows that the discontinuity between the rotating and stationary walls creates at worst a Dirac delta function forcing at the discontinuity. It is difficult to analytically compute the flow at the junction between the rotating and stationary walls. The purpose of this section is to show that when calculating the main features of the global

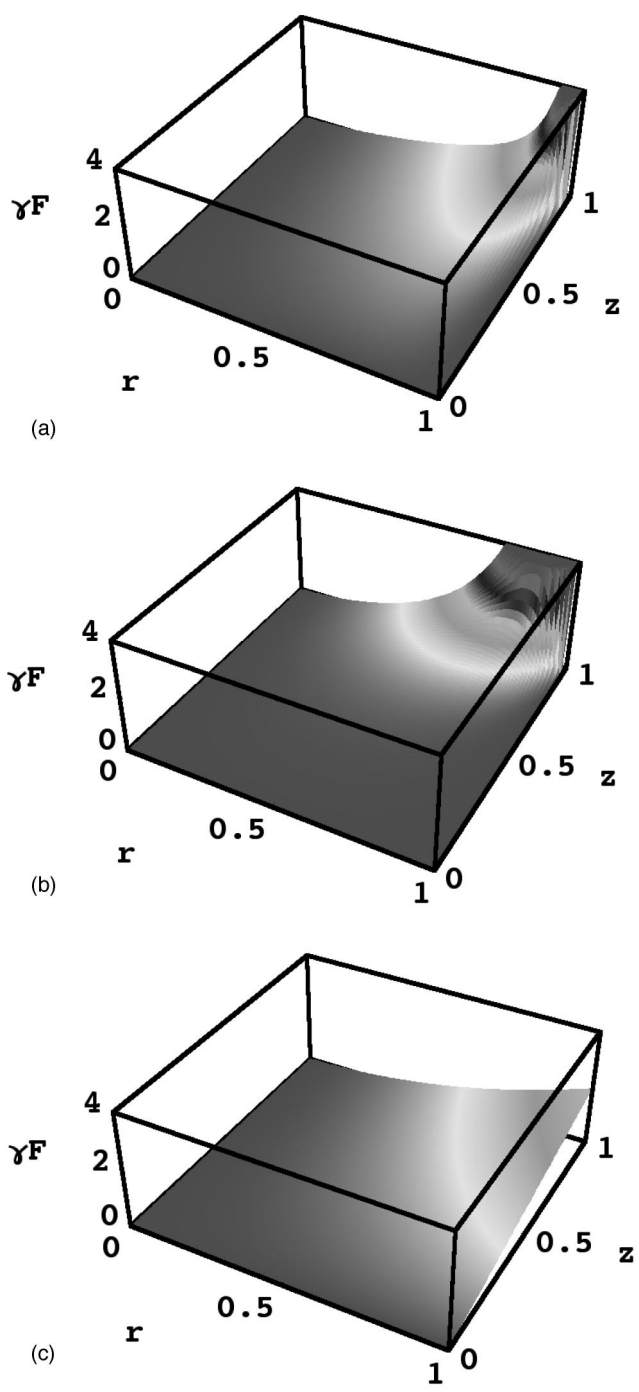


FIG. 4. (a) The forcing function for the secondary flow for an aspect ratio $\gamma=0.25$ with a stationary end wall. (b) The forcing function for the secondary flow for an aspect ratio $\gamma=1$ with a stationary end wall. (c) The approximate small aspect ratio forcing function for the secondary flow.

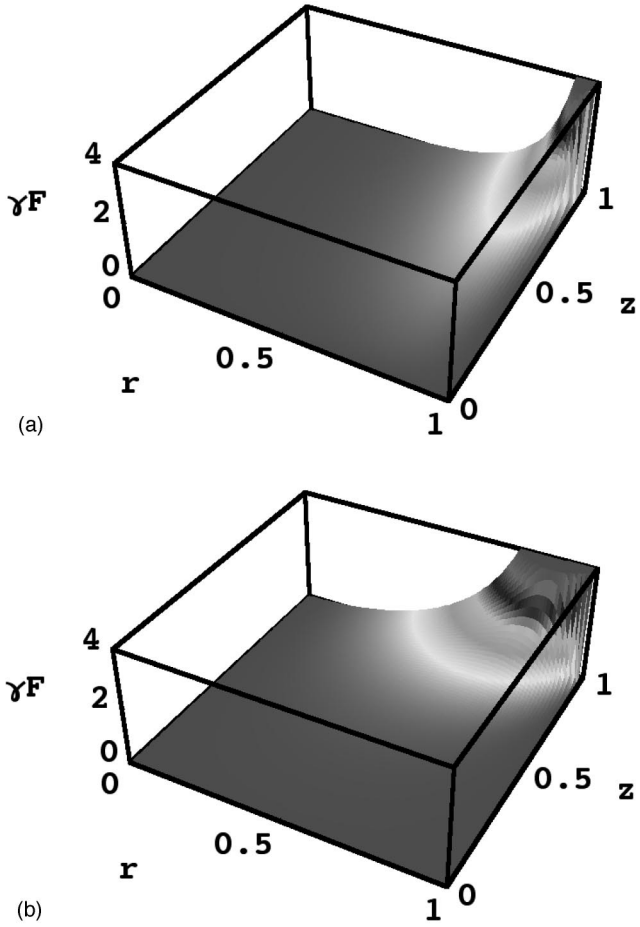


FIG. 5. (a) The forcing function for the secondary flow for an aspect ratio $\gamma=0.25$ with a free surface. (b) The forcing function for the secondary flow for an aspect ratio $\gamma=1$ with a free surface.

$$F_{0,fix}=\frac{1}{\gamma}\frac{\partial u^2_{\theta,0,fix}}{\partial z}=\frac{2}{\gamma}\left(rz+2\sum_{n=1}^{\infty}\frac{\sin[n\pi(z-1)]}{n\pi}\frac{I_1[n\pi r/\gamma]}{rI_1[n\pi/\gamma]}\right)\times\left(r+2\sum_{n=1}^{\infty}\cos[n\pi(z-1)]\frac{I_1[n\pi r/\gamma]}{rI_1[n\pi/\gamma]}\right). \tag{14}$$

flow field at low Reynolds number in a small aspect ratio geometry, the conditions at the discontinuity can be neglected with a no-slip boundary condition opposite the rotating end wall and that the conditions at the discontinuity cannot be neglected with a free-slip boundary condition opposite the rotating end wall.

The forcing function with one stationary end wall, $F_{0,fix}$, is

This forcing function diverges. The convergence properties are worst at the discontinuity between the rotating and stationary walls. At the rotating outer wall, the most singular part of the forcing function is formally the product of a Dirac delta function and a Heaviside function.

To examine the properties of the forcing function at the boundary discontinuity, and so check whether a reasonable solution to the first-order flow can be obtained Lanczos factors need to be used. Using Lanczos factors, the forcing function with a stationary end wall is

$$F_{0,fix} = \frac{2}{\gamma}\left( rz + 2\sum_{n=1}^{k} \frac{\sin[n\pi(z-1)]}{n\pi} \frac{\sin[n\pi/k]}{n\pi/k} \frac{I_1[n\pi r/\gamma]}{rI_1[n\pi/\gamma]} \right) \times \left( r + 2\sum_{n=1}^{k} \cos[n\pi(z-1)] \frac{\sin[n\pi/k]}{n\pi/k} \frac{I_1[n\pi r/\gamma]}{rI_1[n\pi/\gamma]} \right). \tag{15}$$

The forcing function is now a meaningful finite sum. Forcing functions for aspect ratios of 0.25 and 1 are shown in Figs. 4(a) and 4(b). These figures are scaled so that the maximum value of each forcing function does not appear so that other features of the forcing function away from the discontinuity can be distinguished. These forcing functions were calculated using 30 terms in each series. By using 15 terms in each series, no significant quantitative change in the forcing functions was found except at the discontinuity. From these figures one observes that at the transition between the rotating and stationary walls, the forcing function has a large positive value which, when a large number of terms are used in the series representation, approaches a Dirac delta function. Figure 4(c) shows the approximate forcing function determined using the intermediate asymptotic flow field representation for a flow with a stationary end wall, $2r^2z/\overline{\gamma}$, for an aspect ratio of 1. It is quantitatively similar to the forcing function at an aspect ratio of 0.25 [Fig. 4(a)] and qualitatively similar at an aspect ratio of 1 [Fig. 4(b)]. The approximate forcing function differs from the exact forcing functions at the boundary discontinuity, where the exact forcing functions have a large magnitude spike. The approximate forcing function also differs from the exact forcing function at the outer stationary wall where the exact forcing function is zero but the approximate forcing function has a finite value. For small aspect ratios, the approximate forcing function, which does not depend on the conditions at the discontinuity, is the dominant component of the forcing function.

With a free surface, the series expansion for the forcing function is also not a meaningful expression because of the discontinuity between the rotating end wall and the stationary sidewall. Using Lanczos correction factors, the forcing function is

$$F_{0,free} = \frac{1}{\gamma}\frac{\partial u^2_{\theta,0,free}}{\partial z} = \left( r + \sum_{n=0}^{k} \frac{2I_1[(n+1/2)\pi r/\gamma]}{I_1[(n+1/2)\pi/\gamma]} \frac{\sin[(n+1/2)\pi(1-z)]}{(n+1/2)\pi} \frac{\sin[(n+1/2)\pi/k]}{(n+1/2)\pi/k} \right) \times \frac{2}{\gamma}\left( -\sum_{n=0}^{k} \frac{2I_1[(n+1/2)\pi r/\gamma]}{I_1[(n+1/2)\pi/\gamma]} \frac{\sin[(n+1/2)\pi/k]}{(n+1/2)\pi/k} \cos[(n+1/2)\pi(1-z)] \right). \tag{16}$$

This forcing function is plotted in Figs. 5(a) and 5(b) for aspect ratios of 0.25 and 1. The forcing function is evaluated using 30 term in each series. In a similar manner to the forcing function with a stationary end wall, it was found that by using 15 terms in each series, no qualitative change in the forcing functions occurred. At small aspect ratio, Fig. 5(a) shows that the forcing function is close to zero everywhere apart from near the stationary sidewall. This behavior is very different from the forcing function in Fig. 4(a) for an apparatus with a stationary end wall opposite the rotating end wall because with a free surface the small aspect ratio intermediate asymptotic similarity solution, $r$, does not contribute to the axial derivative of the velocity field. Figure 5(b), which is for an aspect ratio of 1, is similar to Fig. 4(b) for which the free surface is replaced by a no-slip boundary condition. These figures show that in a small aspect ratio geometry with a free surface, all components of the forcing function depend on the conditions at the corner discontinuity.

### E. Solution for the first-order flow field at small aspect ratio with a fixed end wall

To show that the conditions at the corner discontinuity are unimportant in determining the global structure of the flow field, a similarity solution for the first-order flow field is computed using the approximate small aspect ratio azimuthal velocity field for an apparatus with a stationary end wall, $rz$, in the forcing function. The similarity solution does not satisfy all the appropriate experimental boundary conditions discussed in Sec. III A. A solution that satisfies the boundary conditions is obtained by using a series expansion.

Using the approximate forcing function, the equations to be solved are

$$\frac{2r^2z}{\gamma} = D^2D^2\Psi_{1,fixed}, \quad u_{\theta,1,fixed} = 0. \tag{17}$$

Schulz-Grunow[13] and Pao[12] showed that a particular solution for the first-order stream function, $\Psi_{1,fixed,p}$, which satisfies the forcing function, the no-slip and no-flux boundary conditions on the top and bottom walls but does not satisfy the no-slip and no-flux boundary conditions on the outer stationary wall, is

$$\Psi_{1,fixed,p} = \gamma^3 r^2 \left( \frac{z^5}{60} - \frac{z^3}{20} + \frac{z^2}{30} \right). \tag{18}$$

A plot of the similarity solution stream function is shown in Fig. 6(a) for an aspect ratio of 0.25.

The boundary conditions on the outer stationary wall can be satisfied using a biorthogonal series expansion in which the coefficients are obtained using a least-squares procedure as outlined in Appendix B. The solution is

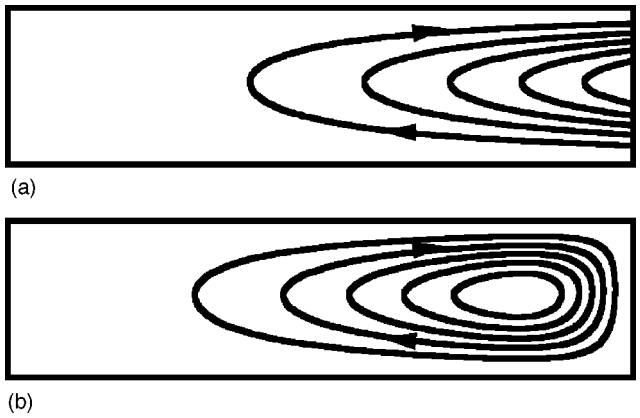


FIG. 6. (a) The similarity solution $\Psi_{1,fixed,p}$ for the stream function for axial and radial fluid motions at an aspect ratio $\gamma=0.25$. Five equally spaced contours are shown. (b) The solution $\Psi_{1,fixed}$ for the stream function for axial and radial fluid motions at an aspect ratio $\gamma=0.25$. Five equally spaced contours are shown.

$$\Psi_{1,fixed} = \gamma^3 r^2\left(\frac{z^5}{60} - \frac{z^3}{20} + \frac{z^2}{30}\right) + \sum_{n=1}^{k} a_n \frac{rI_1[\omega_n r/\gamma]}{I_1[\omega_n/\gamma]}\phi_n[z] + \overline{a}_n \frac{rI_1[\overline{\omega}_n r/\gamma]}{I_1[\overline{\omega}_n/\gamma]}\overline{\phi}_n[z],$$
$$\phi_n[z] = \sin[\omega_n z] + z(\omega_n \cos[\omega_n] - \sin[\omega_n])\frac{\sin[\omega_n z]}{\sin[\omega_n]} - z\omega_n \cos[\omega_n z]. \tag{19}$$

In this equation the constants $\overline{a_n}$ are the complex conjugates of the constants $a_n$, both of which are determined by the least-squares procedure. The eigenvalues $\omega_n$ are chosen to satisfy the no-flux, $\phi_n[0]=\phi_n[1]=0$, and no-slip boundary, $\partial\phi_n[0]/\partial z=\partial\phi_n[1]/\partial z=0$, conditions on the top and bottom walls. These boundary conditions determine a transcendental eigenvalue equation $\cos[2\omega_n]+2\omega_n^2=1$, which is solved numerically. The eigenvalues come in complex conjugate pairs as shown in Fig. 7, so the final expansion gives a real result. A sample stream function is shown in Fig. 6(b) using 75 terms in the series expansion. With this number of terms, the maximum error in the satisfaction of the no-slip and no-flux boundary conditions on the outer stationary wall is less than $10^{-8}$. Figure 6 shows that for aspect ratios less than 0.25 and Reynolds numbers less than 1, the similarity solution $\Psi_{1,fixed,p}$ is an intermediate asymptotic representation of the velocity field because the effects of the sidewall are limited to a small region in which the flow is turned around. Furthermore, because the biorthogonal system is complete, similar results will hold for any flow where the Reynolds number and aspect ratio are much less than 1 and there is no net volume flux at the edge of the disks.

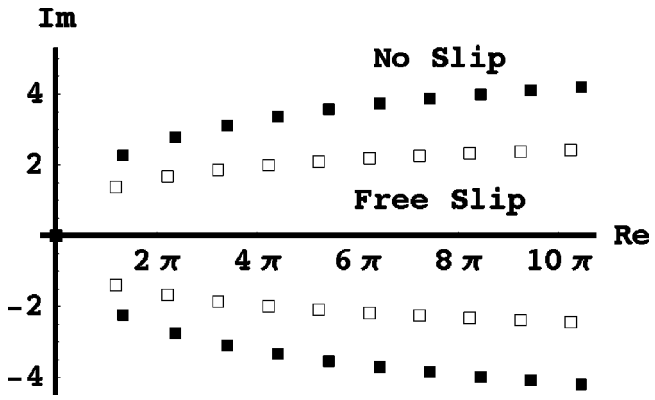


FIG. 7. The spectra of the operator for the axial eigenfunctions with both free-slip and no-slip boundary conditions opposite the rotating end wall. Im denotes the imaginary axis and Re denotes the real axis.

It is surprising that the flow does not have Moffat corner vortices because a computation at a Reynolds numbers of 50 for an aspect ratio of 0.5 does.[18] This can be explained. For the small aspect ratio asymptotic forcing function considered here, the particular solution $\Psi_{1b}$ decays at a rate proportional to $r^2$ with distance from the sidewall, while the homogeneous series solution decays exponentially with distance from the sidewall (for large argument the modified Bessel function is asymptotic to[32] $I_1[r\omega]\sim\exp[r\omega]/\sqrt{r\omega}$). The Bessel function decay is rapid because even though the eigenvalues are complex, the spectrum in Fig. 7 shows that they have much larger real components than imaginary components, and so the oscillations they create decay rapidly. Thus, the particular solution dominates throughout the whole flow field and no Moffat eddies are seen. If the exact forcing function were to be used, Moffat vortices would be seen because the forcing function is zero at the stationary outer wall and then increases rapidly towards the interior before beginning to decrease again as shown in Fig. 4(a). Thus at the junction between the stationary end wall and the sidewall, the homogeneous solutions would dominate.

### F. Asymptotic solution structure for the first-order flow field at small aspect ratio with a free surface

The forcing function for the secondary flow with a free surface Eq. (17) is complicated. As observed by Hills,[26] to obtain a theoretical understanding of the behavior for small aspect ratio geometries, only the dominant component of the forcing function at large distances from the stationary sidewall needs to be examined. A simplified model for the first-order correction flow field, $\Psi_{1,free}$, using the dominant component of the forcing function when the aspect ratio is much less than 1 is

$$\Lambda\frac{4r}{\gamma}\frac{I_1[\pi r/2\gamma]}{I_1[\pi/2\gamma]}\cos[\pi(1-z)/2] = D^2D^2\Psi_{1,free},\ u_{\theta,1,free}=0. \tag{20}$$

In this equation, $\Lambda=2k\sin[\pi/2k]/\pi$ is a constant that depends on the number of terms used in the Lanczos series expansion and hence is explicitly determined by the conditions at the corner discontinuity. When a large number of terms in the series expansion are used $\Lambda\approx 1-\pi^2/24k^2$, the limit of $\Lambda=1$, is never reached because this corresponds to discontinuous boundary conditions which would not exist in an experiment.

To show that the single term of the forcing function in Eq. (20) is a good representation of the forcing function away from the starionary sidewall note that for large argument the modified Bessel function is asymptotic to[32] $I_1[(n+1/2)\pi r/\gamma] \sim \exp[(n+1/2)\pi r/\gamma]/\sqrt{(n+1/2)\pi r/\gamma}$. Thus the first mode of the forcing function is the dominant mode of the forcing function and so will determine the dominant mode of the particular solution when $\gamma \ll 1$ and when $r < 1-\gamma$. By obtaining a solution to this equation, it will be possible to determine if the particular or the homogeneous solutions dominate for large distances from the stationary sidewall. Assuming a particular solution $\Psi_{1,free,p}$ of the form

$$\Psi_{1,free,p} = \Lambda \frac{rI_1[\pi r/2\gamma]}{I_1[\pi/2\gamma]} F[z], \tag{21}$$

it is found that

$$4\gamma^3 \cos[\pi(1-z)/2] = (\pi/2)^4 F[z] + 2(\pi/2)^2 d^2F[z]/dz^2 + d^4F[z]/dz^4. \tag{22}$$

Solving this differential equation and satisfying all the boundary conditions except those at the stationary sidewall, the following particular solution is obtained:

$$\Psi_{1,free,p} = \frac{2\Lambda\gamma^3 r}{\pi^2(\pi^2-4)} \frac{I_1[\pi r/2\gamma]}{I_1[\pi/2\gamma]} \{2\pi z \cos[\pi z/2] + (1-z)[(\pi^2-4)z-4]\sin[\pi z/2]\}. \tag{23}$$

In a similar manner to the flow with a no-slip boundary condition opposite the rotating end wall, the boundary conditions at the stationary sidewall can be satisfied using a biorthogonal series expansion,

$$\Psi_{1,free} = \Psi_{1,free,p} + \sum_{n=1}^{k} b_n \frac{rI_1[\varpi_n r/\gamma]}{I_1[\varpi_n/\gamma]} \varphi_n[z] + \overline{b}_n \frac{rI_1[\overline{\varpi}_n r/\gamma]}{I_1[\overline{\varpi}_n/\gamma]} \overline{\varphi}_n[z],$$
$$\varphi_n[z] = z\sin^2[\varpi_n]\cos[\varpi_n z] + (z\varpi_n - z\sin[\varpi_n]/2 - \varpi_n)\sin[\varpi_n z]. \tag{24}$$

The constants $b_n$ can be determined through a least squares procedure just like for the flow with no-slip boundary conditions opposite the rotating end wall. The eigenvalues $\overline{\omega}_n$ are chosen to satisfy the no-slip boundary conditions on the rotating end wall and the free-slip boundary conditions on the free surface. The eigenvalues satisfy the transcendental equation $2\overline{\omega}_n = \sin[2\overline{\omega}_n]$, and so must be calculated numerically. The spectrum is shown in Fig. 7, and in a similar manner to the spectrum with a no-slip boundary condition opposite the rotating end wall, the eigenvalues come in complex conjugate pairs, so the final expansion for the streamfunction is real.

The important question is whether the homogeneous or particular solution dominates at large distances from the stationary sidewall. This is determined by the size of the slowest decaying component of the homogeneous solution and hence only the knowledge of the size of the real components of the smallest eigenvalues used is required. The eigenvalue of zero is associated with polynomial solutions, none of which are required to obtain the full solution to the differential equation. The next smallest pair of eigenvalues is $3.75 \pm 1.38i$. These eigenvalues have a real component that is larger than $\pi/2 \approx 1.57$, the eigenvalue that determines the decay of the particular solution. Thus, the slowest decaying component of the particular solution decays slower than the slowest decaying component of the homogeneous solution. The asymptotic structure of the flow far away from the stationary sidewall is therefore determined by a similarity solution of the first kind, which is itself very dependent on the conditions at the corner discontinuity.

### G. Using Lanczos factors to examine the effect of the discontinuity on the torque

By using the Lanczos factors it is possible to examine how the torque depends on the conditions at the discontinuity. The total torque on the upper rotating lid for a flow with a stationary end wall, $T$, is examined although analogous results can be obtained for a flow with a free surface opposite the rotating end wall:

$$T = 2\pi \int_0^1 \left.\frac{\partial u_{\theta,0}}{\partial z}\right|_{z=1} r^2 dr = \frac{\pi}{2} + \sum_{i=1}^{k} \frac{4\gamma}{n} \frac{I_2[n\pi/\gamma]}{I_0[n\pi/\gamma]} \frac{\sin[n\pi/k]}{n\pi/k}. \tag{25}$$

The Lanczos factors provide a means of setting a minimum resolvable scale. By increasing the number of terms in the series expansion, one can decrease the effective size of the gap between the rotating lid and the stationary sidewall. Figure 4 shows that as the number of terms in the series expansion is increased (this corresponds to a decrease in the gap width) the torque increases logarithmically without bound. This confirms Schmiedens'[8] result that the total torque on the rotating lid in Stokes flow with discontinuous boundary conditions is unbounded and has a sensitive dependence on the conditions at the boundary between the stationary sidewall and rotating lid.

Other researchers[12] have suggested that it is possible to estimate the torque by neglecting the contribution from the discontinuity. This can be accomplished by integrating almost all the distance along the rotating lid but stopping the integration a little before the discontinuity. Torques with upper integration limits of 90% and 99% of the lid radius are shown in Fig. 8. Although both these series converge to a limit when a large number of terms in the Lanczos modified series expansion are used, they do not converge to the same limit; thus the torque that must be exerted on the entire rotating lid cannot be determined without a detailed description of the conditions at the discontinuity in the Stokes limit. If the torque is measured on a portion of the rotating lid that is far from the corner discontinuity, the continuum estimate is accurate at small Reynolds numbers. Figure 8 shows that this estimate is insensitive to the conditions at the discontinuity provided enough terms in the series are used. This is because

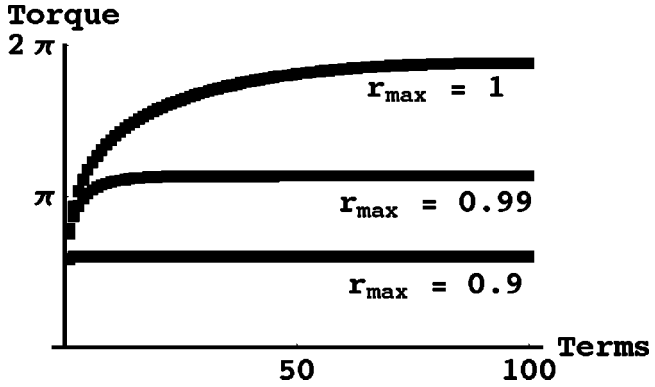


FIG. 8. The torque on the rotating lid for a cavity with a stationary end wall as a function of the number of terms in a Lanczos modified series expansion and the upper radial integration limit. The apparatus has an aspect ratio $\gamma = 0.25$.

by increasing the number of terms in the series, the effective gap width decreases but the torque measured away from the discontinuity remains constant.

The present study confirms Schmeidens'[8] result that the torque in Stokes flow with discontinuous boundary conditions is logarithmically divergent. This is due to a subtle failure in the uniform validity of the perturbation series. Formally, the scaling requirement that $|\mathbf{u}_n| \gg \mathrm{Re}|\mathbf{u}_n \cdot \nabla \mathbf{u}_n|$ is not violated because even though the Stokes flow has discontinuous boundary conditions (and so, $\partial u_{\theta,0}/\partial z$ is unbounded at the discontinuity), the magnitude of the neglected inertial terms, $\mathbf{u}_0 \cdot \nabla \mathbf{u}_0 = 0$, is still less than the Stokes terms because the zeroth-order axial and radial velocities are zero. However, a small zeroth-order boundary perturbation can make the zeroth-order axial and radial flows not equal to zero, for which the scaling requirement $|\mathbf{u}_0| \gg \mathrm{Re}|\mathbf{u}_0 \cdot \nabla \mathbf{u}_0|$ is violated because $u_{z,0}\partial u_{\theta,0}/\partial z$ is unbounded at the discontinuity. This indicates that if discontinuous boundary conditions were to hold in an experiment, inertial effects would be important near the corner even at arbitrarily small Reynolds numbers. Lugt and Haussling[21] examined the torque in numerical simulations of this flow, but their grid spacing was too coarse to resolve the flow at the corner discontinuity. Simulations that fully resolve the flow near the corner discontinuity and examine its sensitivity to boundary perturbations are required to determine the behavior of the torque in the limit of discontinuous boundary conditions.

## IV. DISCUSSION

The present study shows that as found by Hills,[26] because the primary small Reynolds number flow field has only an azimuthal component, the first-order correction to the primary flow field has a determining influence on the small Reynolds number axial and radial velocity fields.

Hills[26] showed that for a semi-infinite cylindrical lid-driven cavity, the primary azimuthal flow field decayed exponentially with distance from the rotating end wall. This is in agreement with the results from this study where in a large aspect ratio geometry the primary azimuthal flow is concentrated near the rotating end wall.

The Stokes flow solution for a semi-infinite cavity obtained by Hills,[26] $u_{\theta,0,\mathrm{Hills}}$, can be derived from the finite length Stokes solutions for flow with a fixed surface opposite the rotating end wall.[12] Using a transformed axial coordinate, $\hat{z} = (1-z)\gamma$, in which the center of the rotating lid is at the origin, the Stokes solution for a semi-infinite cavity is

$$u_{\theta,0,\mathrm{Hills}} = \sum_{n=1}^{\infty} \frac{-2J_1[\lambda_n r]\exp[-\lambda_n \hat{z}]}{\lambda_n J_0[\lambda_n]}. \tag{26}$$

The solution with a free surface opposite the rotating end wall, Eq. (11), can also be reduced to Hills' solution. Using the axial coordinate transformation, the Stokes flow field for a finite size cylindrical lid driven cavity Eq. (11) becomes

$$u_{\theta,0,fix} = \sum_{n=1}^{\infty} \frac{-2}{\lambda_n} \frac{\cosh[(\gamma-\hat{z})\lambda_n]}{\cosh[\gamma\lambda_n]} \frac{J_1[\lambda_n r]}{J_0[\lambda_n]}. \tag{27}$$

Since a semi-infinite cylinder corresponds to the aspect ratio becoming large, by using the asymptotic limit for the hyperbolic cosine function with large argument,

$$\cosh[(\gamma-\hat{z})\lambda_n]/\cosh[\gamma\lambda_n] \approx \exp[(\gamma-\hat{z})\lambda_n]/\exp[\gamma\lambda_n] = \exp[-\hat{z}\lambda_n], \tag{28}$$

Hills' solution, Eq. (26), is obtained as a limiting case of large aspect ratio.

For the semi-infinite cavity, Hills'[26] calculation shows the existence of a sequence of eddies that decay with distance from the end wall. The structure of the eddies is determined by the slowest decaying homogeneous solutions of the partial differential equation for the stream function. The present study shows that in a small aspect ratio apparatus with a stationary end wall and with a free surface, the asymptotic structure of the secondary flow away from the stationary sidewall is determined by the particular solution of the partial differential equation for the stream function. Comparing these results to studies of the rectangular lid-driven cavity[15] suggests that as the aspect ratio of a cylindrical lid-driven cavity with a fixed end wall is increased, the number of eddies also increases. Thus, there must be a swap between dominance of the flow topology by the particular solution (a similarity solution of the first kind) to dominance by the homogeneous solutions (a similarity solution of the second kind) in both the Stokes flow field and the first-order inertial correction to the Stokes flow field.

Lopez *et al.*[17] found that for a flow with free-slip boundary conditions in a small aspect ratio geometry, the flat free-slip boundary condition gives a poor approximation to the flow field because it imposes an additional axial symmetry that does not exist in an experiment. The spectra for the homogeneous solutions of the stream function with free-slip and no-slip boundary conditions, Fig. 7, are similar. While the results obtained here are only correct at small Reynolds number, they suggest that the stress free boundary condition is less important in determining the flow field after the primary instability than the surface curvature effect and the effect of other boundary perturbations on conditions near the corner discontinuity.

Hills and Moffat[33] and Moffat and Duffy[34] have found that inertial effects can be significant for arbitrarily small Reynolds numbers in Jeffery–Hamel and scarping disk flows. In the flow studied by Hills and Moffat,[33] the effect of the corner discontinuity on the global flow field was locally limited for Reynolds numbers less than 1. Moffat and Duffy[34] found that by changing the opening angle in a Jeffrey–Hamel flow, they could make inertial effects at the source important throughout the flow field for arbitrarily small source Reynolds numbers. Dennis *et al.*[35] also studied Jeffery-Hamel flow in a finite geometry for which the Stokes solution was uniformly valid at small Reynolds numbers. At large Reynolds numbers however, Dennis *et al.*[35] found that slight asymmetries at the source can determine the structure of the global flow field.

In Sec. III G of the present study, it was shown that the local flow field near the discontinuity in a cylindrical cavity with a rotating end wall is sensitive to small boundary perturbations that can make inertial effects locally important. For Reynolds numbers less than 1, with a no-slip boundary condition opposite the rotating end wall, inertia only affects a limited portion of the flow field—this is similar to what Hills and Moffat[33] found. At large Reynolds numbers, however, the corner discontinuity is a strong localized source of vorticity, and so may be important in determining the global flow structure—this is similar to what Dennis *et al.*[35] found. Hartnack, Brons, and Spohn,[5] Thompson and Hourigan,[22] and Ventikos[23] have shown experimentally and numerically that boundary perturbations can change the internal structure of a vortex breakdown bubble for aspect ratios close to 1. Mellor, Chapple, and Stokes[7] also observe that if there is a small gap between a stationary sidewall and the top and bottom walls, then for aspect ratios much less than 1 there is circulation out of the gap between the rotating end walls and into the gap between the stationary sidewall and stationary end wall. They show that with a free edge boundary condition, the flow between the disks is very different from that when there is a stationary sidewall. It therefore seems plausible that by preventing circulation out of the corner discontinuity when there is a fixed sidewall, one could also change the internal flow structure. Brady and Durlofsky[6] have suggested that the conditions at the edges of the disks determine the asymptotic flow structure and that the asymptotic flow structure is particularly sensitive to asymmetric perturbations. What needs to be experimentally investigated is how carefully the conditions need to be specified to determine the asymptotic flow towards the center of the disks.

With a free-slip boundary condition opposite the rotating end wall and for Reynolds numbers less than 1, the sensitivity of the flow field near the discontinuity to small perturbations is important because at small aspect ratio the conditions near the discontinuity determine the global axial and radial flow structure. Spohn *et al.*[3] observed that the global flow structure at small aspect ratios is sensitive to ground vibrations. Since vibrations will change the spacing between the rotating disk and the stationary sidewall, it is not surprising that they change the global flow structure.

It is well known that for Reynolds numbers greater than 1, flows in cavities with discontinuous boundary conditions often have several different solutions.[15] The flow in a small aspect ratio cavity with a rotating end wall is also known to have many possible solutions if the conditions at the edge of the disks are not carefully specified.[6,7] It seems plausible that by changing the conditions at the discontinuity one may control the internal structure of the large Reynolds number flow between a rotating and a stationary disk with a stationary sidewall.

## V. CONCLUSION

The present study has demonstrated that in a small aspect ratio cylindrical cavity with a rotating end wall, a similarity solution of the first kind describes the Stokes flow field with both free-slip and no-slip boundary conditions opposite the rotating end wall. It has also been shown that at small aspect ratio, the first inertial correction is described by a similarity solution of the first kind for both no-slip and free-slip boundary conditions opposite the rotating end wall.

The effect of the boundary discontinuity has been studied using Lanczos factors to allow the trigonometric series expansion to be differentiated. It has been confirmed that the flow field near the discontinuity is important in determining the torque for Reynolds numbers less than 1. The present study has demonstrated that the boundary discontinuity is unimportant in determining the global secondary flow structure for Reynolds numbers less than 1 with a no-slip boundary condition opposite the rotating end wall. The present study has also demonstrated that the boundary discontinuity is important in determining the global secondary flow structure for Reynolds numbers less than 1 with a free-slip boundary condition opposite the rotating end wall.

## ACKNOWLEDGMENTS

The author would like to thank Alexander Smits for some helpful comments on earlier versions of this paper. A portion of this study was completed as part of the requirements of a master of science in engineering degree at Princeton University, during which the author was supported by an Upton Fellowship. Another part of this study was completed while on a Ford Foundation fellowship at the African Institute for Mathematical Sciences. The support and constructive criticism received from members of both institutions is gratefully acknowledged.

## APPENDIX A: CALCULATION OF STOKES FLOW FIELDS USING SEPARATION OF VARIABLES

To solve for the Stokes azimuthal velocity field, Eq. (5), with a free surface opposite the rotating end wall, a correction to satisfy the boundary conditions on the stationary sidewall needs to be added to the polynomial similarity solution $r$. The partial differential equation satisfied by the correction velocity field $\tilde{u}_{\theta,0}$ is

$$\frac{1}{\gamma^2}\frac{\partial^2 \tilde{u}_{\theta,0}}{\partial z^2}+\frac{1}{r}\frac{\partial \tilde{u}_{\theta,0}}{\partial r}+\frac{\partial^2 \tilde{u}_{\theta,0}}{\partial r^2}-\frac{\tilde{u}_{\theta,0}}{r^2}=0. \tag{A1}$$

This has boundary conditions

$$\tilde{u}_{\theta,0}[1,z] = -1,\ \tilde{u}_{\theta,0}[r,1] = \frac{\partial \tilde{u}_{\theta,0}}{\partial z}[r,0] = 0. \tag{A2}$$

Assume a series solution of the form

$$\tilde{u}_{\theta,0} = \sum_{n=1}^{\infty} \sin[(n+1/2)\pi(z-1)]R[r]. \tag{A3}$$

Substituting this series solution into the differential equation and taking the inner product with $\sin[(m+1/2)\pi(z-1)]$, an ordinary differential equation for the radial component is obtained:

$$-\frac{(m+1/2)^2\pi^2}{\gamma^2}R_m + \frac{1}{r}\frac{dR_m}{dr} + \frac{d^2R_m}{dr^2} - \frac{R_m}{r^2} = 0. \tag{A4}$$

The two solutions to this equation are the modified Bessel functions of the first and second kind of order one, $I_1[(m+1/2)\pi r/\gamma]$ and $K_1[(m+1/2)\pi r/\gamma]$. Since the solution needs to be finite along the central axis of the cavity, only the modified Bessel function of the first kind is allowed. The transformed boundary condition is

$$R_m[(m+1/2)\pi/\gamma] = \frac{-\int_0^1 \sin[(m+1/2)\pi(z-1)]dz}{\int_0^1 \sin^2[(m+1/2)\pi(z-1)]dz} = \frac{2}{(m+1/2)\pi}. \tag{A5}$$

The full solution is then given by

$$u_{\theta,0,free} = r + 2\sum_{n=0}^{\infty} \frac{I_1[(n+1/2)\pi r/\gamma]}{I_1[(n+1/2)\pi/\gamma]} \times \frac{\sin[(n+1/2)\pi(z-1)]}{(n+1/2)\pi}. \tag{A6}$$

The solution to Eq. (5) with a free surface opposite the rotating end wall can also be expressed using an alternative basis of orthogonal functions. If no similarity solution is used, the appropriate boundary conditions are

$$u_{\theta,0}[r,1] = r,\quad \frac{\partial u_{\theta,0}}{\partial z}[r,0] = u_{\theta,0}[1,z] = 0. \tag{A7}$$

Assume a separable solution in terms of regular Bessel functions of the first kind of order 1:

$$u_{\theta,0} = \sum_{n=1}^{\infty} J_1[\lambda_n r]Z[z]. \tag{A8}$$

The boundary condition at $r=1$ determines the eigenvalues $\lambda_n$ as the $n$th zero of the regular Bessel function of the first kind of order 1. Substituting this series solution into the differential equation and taking the inner product with $J_1[\lambda_m r]$, using the weighting function $r$, an ordinary differential equation for each axial component is obtained:

$$\frac{1}{\gamma^2}\frac{d^2Z_m}{dr^2} - \lambda_m^2 Z_m = 0. \tag{A9}$$

The solutions to this differential equation are $\sinh[\lambda_m \gamma z]$ and $\cosh[\lambda_m \gamma z]$. To determine the linear combination of these solutions, the transformed boundary conditions

$$\frac{\partial Z_m}{\partial z}[0] = \frac{\int_0^1 0 * rJ_1[\lambda_m r]dr}{\int_0^1 rJ_1^2[\lambda_m r]dr} = 0,\qquad Z_m[1] = \frac{\int_0^1 r^2 J_1[\lambda_m r]dr}{\int_0^1 rJ_1^2[\lambda_m r]dr} = \frac{-2}{\lambda_n J_0[\lambda_n]} \tag{A10}$$

are required. Only $\cosh[\lambda_m \gamma z]$ satisfies the boundary condition at $z=0$, thus the full solution is

$$u_{\theta,0,fix} = \sum_{n=1}^{\infty} \frac{-2}{\lambda_n}\frac{\cosh[\gamma z\lambda_n]}{\cosh[\gamma\lambda_n]}\frac{J_1[\lambda_n r]}{J_0[\lambda_n]}. \tag{A11}$$

## APPENDIX B: CALCULATION OF FIRST-ORDER FLOW FIELD USING A SERIES EXPANSION

To obtain a solution for the first-order flow field a biorthogonal series expansion is used. Only an outline of the method is provided here and further details can be found in Refs. 26 and 36–39. The partial differential equation to be satisfied by the homogeneous stream function is

$$D^2D^2\Psi_{1h} = 0 \tag{B1}$$

with boundary conditions,

$$\Psi_{1h}[r,1] = \Psi_{1h}[r,0] = \Psi_{1h}[0,z] = 0,\qquad \frac{\partial \Psi_{1h}}{\partial z}[r,1] = \frac{\partial \Psi_{1h}}{\partial z}[r,0] = 0,\qquad \Psi_{1h}[1,z] = -\gamma^3\left(\frac{z^5}{60} - \frac{z^3}{20} + \frac{z^2}{30}\right),\qquad \frac{\partial \Psi_{1h}}{\partial r}[1,z] = -\gamma^3\left(\frac{z^5}{30} - \frac{z^3}{10} + \frac{z^2}{15}\right),\qquad \frac{\partial \Psi_{1h}}{\partial r}[0,z] < \infty. \tag{B2}$$

Assuming a separable solution of the form $rI_1[\omega_n r/\gamma]\phi_n[z]/I_1[\omega_n/\gamma]$, it is found that $\phi_n[z]$ satisfies the differential equation

$$\frac{\partial^4 \phi_n[z]}{\partial z^4} + 2\omega_n^2\frac{\partial^2 \phi_n[z]}{\partial z^2} + \omega_n^4\phi_n[z] = 0, \tag{B3}$$

with boundary conditions,

$$\phi_n[1] = \phi_n[0] = \frac{\partial \phi_n}{\partial z}[1] = \frac{\partial \phi_n}{\partial z}[0] = 0. \tag{B4}$$

In a domain symmetric about the origin, the solutions of this equation lead to the Papkovich–Fadle functions. However, rather than decompose the boundary condition into symmetric and antisymmetric parts, because of the choice of coordinates, it is better to use a single eigenfunction,

$$\phi_n[z] = \sin[\omega_n z] + z(\omega_n\cos[\omega_n] - \sin[\omega_n])\frac{\sin[\omega_n z]}{\sin[\omega_n]} - z\omega_n\cos[\omega_n]. \tag{B5}$$

For the boundary conditions to be satisfied, the eigenvalues need to solve $\cos[2\omega_n]+2\omega_n^2=1$. This is a transcendental equation with complex roots. The roots can be found numerically and the first ten roots in the right half plane and their complex conjugates are plotted in Fig. 7. The roots are symmetric about the real and imaginary axes, but because of the symmetry of the Bessel and trigonometric functions, only the roots in the right half plane need to be used.

It can be shown that Eq. (B3) satisfies a biorthogonality condition, which can be used to determine the coefficients for the series.[34,36–39] The boundary conditions at $r=1$ have no net flux, and so they satisfy the compatibility[38,39] condition $\int_0^1 \partial\Psi_{1h}[1,z]/\partial r\, dz=\int_0^1 \Psi_{1h}[1,z]dz=0$; this ensures that the biorthogonal series expansion can represent the specified boundary conditions.[39] However, use of the biorthogonality relationship to determine the series expansion constants either leads to an infinite system of coupled linear equations that is difficult to solve[38] or requires the numerical evaluation of an integral with infinite limits that cannot be determined in closed form.[39] Thus while the biorthogonality conditions ensure that a infinite series expansion can converge to the correct solution, the most efficient method of determining the constants is a least squares approach.[36–38] The approximation problem is

$$\begin{pmatrix} -\gamma^3\left(\frac{z^4}{12}-\frac{3z^2}{20}+\frac{z}{15}\right) \\ -\gamma^3\left(\frac{z^5}{30}-\frac{z^3}{10}+\frac{z^2}{15}\right) \end{pmatrix} = \sum_{n=1}^{k} \begin{pmatrix} a_n\frac{\partial\phi_n}{\partial z}[z]+\overline{a_n}\frac{\partial\overline{\phi_n}}{\partial z}[z] \\ a_n\phi_n[z]+\overline{a_n}\overline{\phi_n}[z] \end{pmatrix}. \tag{B6}$$

The boundary condition for the stream function has been changed to a boundary condition for the axial derivative of the stream function to ensure that the inner product for the approximation problem is dimensionally consistent, as described by Trefethen and Embree.[38] The least squares problem is to determine the coefficients $a_n$ that minimize the square of the error in the satisfaction of the boundary conditions at $k$ equally spaced points in the axial direction. This gives twice as many points as coefficients, and so allows for a better approximation of the true solution than choosing the same number of points as coefficients without excessive computation. The overdetermined linear system of equations is then solved by QR factorization.[38]


[1] M. P. Escudier, "Observations of the flow produced in a cylindrical container by a rotating end-wall," Exp. Fluids **2**, 189 (1984).
[2] A. Spohn, M. Mory, and E. J. Hopfinger, "Experiments on vortex breakdown in a confined flow generated by a rotating disc," J. Fluid Mech. **370**, 73 (1998).
[3] A. Spohn, M. Mory, and E. J. Hopfinger, "Observations of vortex breakdown in an open cylindrical container with a rotating bottom," Exp. Fluids **14**, 70 (1993).
[4] H. J. Lugt and M. Abboud, "Axisymmetric vortex breakdown with and without temperature effects in a container with a rotating lid," J. Fluid Mech. **179**, 179 (1987).
[5] J. N. Hartnack, M. Brons, and A. Spohn, "The role of asymmetric perturbations in steady vortex breakdown bubbles," Technical University of Denmark, DCAMM Report No. 628, 2000.
[6] J. F. Brady and L. Durlofsky, "On rotating disk flow," J. Fluid Mech. **175**, 363 (1987).
[7] G. L. Mellor, P. J. Chapple, and V. K. Stokes, "On the flow between a rotating and a stationary disk," J. Fluid Mech. **31**, 95 (1968).
[8] C. Schmeiden, "Über den Widerstand einer in einer Flüssigkeit rotierenden Scheibe," Z. Angew. Math. Mech. **8**, 460 (1928).
[9] R. L. Panton, *Incompressible Flow* (Wiley, New York, 1996).
[10] A. Khalili and H. J. Rath, "Analytical solution for a steady flow of enclosed rotating disks," ZAMP **45**, 670 (1994).
[11] H. P. Pao, "A numerical computation of a confined rotating flow," J. Appl. Mech. **37**, 480 (1970).
[12] H. P. Pao, "Numerical solution of the Navier-Stokes equations for flows in the disk-cylinder system," Phys. Fluids **8**, 4 (1972).
[13] F. Schultz-Grunow, "Der Reibungswiderstand rotierender Scheiben in Gehäusen," Z. Angew. Math. Mech. **15**, 191 (1935).
[14] P. Azerad and E. Bänsch, "Quasi-stability of the primary flow in a cone and plate viscometer," J. Math. Fluid Mech. **6**, 253 (2004).
[15] P. N. Shankar and M. D. Deshpande, "Fluid mechanics in the driven cavity," Annu. Rev. Fluid Mech. **32**, 93 (2000).
[16] V. V. Meleshko, V. S. Malyuga, and A. M. Gomliko, "Steady Stokes flow in a finite cylinder," Proc. R. Soc. London, Ser. A **456**, 1741 (2000).
[17] J. M. Lopez, F. Marques, A. H. Hirsa, and R. Miraghie, "Symmetry breaking in free-surface cylinder flows," J. Fluid Mech. **502**, 99 (2004).
[18] A. Yu Gelfgat, P. Z. Bar-Yoseph, and A. Sloan, "Stability of confined swirling flow with and without vortex breakdown," J. Fluid Mech. **311**, 1 (1996).
[19] N. Tsitverblit, "Vortex breakdown in a cylindrical container in the light of continuation of a steady solution," Fluid Dyn. Res. **11**, 19 (1993).
[20] J. M. Lopez, "Axisymmetric vortex breakdown Part 1. Confined swirling flow," J. Fluid Mech. **221**, 533 (1990).
[21] H. J. Lugt and H. J. Haussling, *IUTAM Symposium on Unsteady Boundary Layers*, edited by E. A. Eichelbrenner (Laval University Press, Quebec, 1971), p. 1366.
[22] M. C. Thompson and K. Hourigan, "The sensitivity of steady vortex breakdown bubbles in confined cylinder flows to rotating lid misalignment," J. Fluid Mech. **496**, 129 (2003).
[23] Y. Ventikos, "The effect of imperfections on the emergence of three-dimensionality in stationary vortex breakdown bubbles," Phys. Fluids **14**, L13 (2002).
[24] M. Brons, L. K. Voigt, and J. N. Sorenson, "Topology of vortex breakdown bubbles in a cylinder with a rotating bottom and a free surface," J. Fluid Mech. **428**, 133 (2001).
[25] A. H. Hirsa, J. M. Lopez, and R. Miraghaie, "Symmetry breaking to a rotating wave in a lid-driven cylinder with a free surface: Experimental observation," Phys. Fluids **14**, L29 (2002).
[26] C. P. Hills, "Eddies induced in cylindrical containers by a rotating end-wall," Phys. Fluids **13**, 2279 (2001).
[27] G. I. Barenblatt, *Scaling, Self-Similarity, and Intermediate Asymptotics* (Cambridge University Press, Cambridge, 1996).
[28] W. M. Deen, *Analysis of Transport Phenomena* (Oxford University Press, New York, 1998).
[29] J. M. Lopez and J. Shen, "An efficient spectral-projection method for the Navier–Stokes equations in cylindrical geometries I. Axisymmetric cases," J. Comput. Phys. **139**, 308 (1998).
[30] A. J. Jerri, "Lanczos like $\sigma$-factors for reducing the Gibbs phenomenon in general orthogonal expansions and other representations," Journal of Computational Analysis and Applications **2**, 111 (2000).
[31] A. Lanczos, *Applied Analysis* (Prentice Hall, Englewood Cliffs, 1956).
[32] C. M. Bender and S. A. Orszag, *Advanced Mathematical Methods for Scientists and Engineers* (Springer, New York, 1999).
[33] C. P. Hills and H. K. Moffat, "Rotary honing: a variant of the Taylor paint-scraper problem," J. Fluid Mech. **418**, 119 (2000).
[34] H. K. Moffat and B. R. Duffy, "Local similarity solutions and their limitations," J. Fluid Mech. **96**, 299 (1980).
[35] S. C. R. Dennis, W. H. H. Banks, P. G. Drazin, and M. B. Zaturska, "Flow along a diverging channel," J. Fluid Mech. **250**, 183 (1997).
[36] P. N. Shankar, "The eddy structure in Stokes flow in a cavity," J. Fluid Mech. **250**, 371 (1993).
[37] P. N. Shankar, "On the use of biorthogonality relations in the solution of some boundary value problems for the biharmonic equation," Curr. Sci. **85**, 975 (2003).
[38] L. N. Trefethen and M. Embree, *Spectra and Pseudospectra: The Behaviour of Nonnormal Matrices and Operators* (Princeton University Press, Princeton, in press).
[39] S. A. Lurie and V. V. Vasiliev, *The Biharmonic Problem in the Theory of Elasticity* (Gordon and Breech, Luxembourg, 1995).